Thermodynamic Modeling of the La-Co-O System

Wei-Wei Zhang[1] · Erwin Povoden-Karadeniz[2] · Huixia Xu[1] · Ming Chen[1]

Abstract A thermodynamic modeling of phase diagrams and thermodynamic properties of the La-Co-O system is presented. Special attention is given to the perovskite $LaCoO_{3-\delta}$ phase, due to its outstanding practical importance. In addition to phase equilibria, defect chemistry and charge disproportionation of lanthanum cobaltite were considered during the modeling and are discussed with respect to their thermo-chemical and electrochemical applications. Two sets of optimized parameters are obtained, one for high charge disproportionation ($2Co^{3+} \rightarrow Co^{2+} + Co^{4+}$) and one for low charge disproportionation. By analyzing both oxygen nonstoichiometry and ion distribution results, it is decided that the parameters for low charge disproportionation will be used in the extensions to multi-component system database (e.g. La-Sr-Co-Fe-O). Calculations with the presented thermodynamic database deliver fundamental materials properties for the optimization of technological materials for industrial applications, including SOFC and oxygen membrane.

Keywords charge disproportionation · La-Co-O · lanthanum cobaltite · perovskite · phase diagram

✉ Ming Chen
  minc@dtu.dk

1 Department of Energy Conversion and Storage, Technical University of Denmark, P.O. Box 49, 4000 Roskilde, Denmark

2 Institute of Materials Science and Technology, Vienna University of Technology, 1040 Vienna, Austria
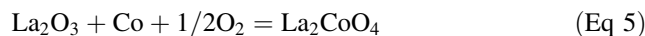
1 Introduction

Perovskite oxides with rare earth or alkaline earth metal on the A site and with 3d transition metal on the B site have drawn a lot of research attentions due to their high catalytic activity and useful electrical and magnetic properties. $LaCoO_{3-\delta}$ is one of those perovskite oxides. It has been shown that lanthanum cobaltite offers high electronic and ionic conductivity, excellent catalytic activity and magnetic property which allow it to be widely used as hydrogenation oxidation catalyst,[1] as SOFC cathode,[2] as oxygen separation membrane and as magneto-hydrodynamic (MHD) electrode.[3]

For most of the above mentioned applications, a successful use of lanthanum cobaltite was however limited by lack of knowledge on phase stability of oxide phases under various operating conditions (temperature and oxygen partial pressure). The La-Co-O system has been investigated previously, with efforts on either experimental determination of thermodynamic or thermochemical properties[4–11] or thermodynamic modeling.[12,13] However, large inconsistency exists between different investigations which makes prediction of materials stability and thermochemical properties in a wide temperature and oxygen partial pressure range difficult.

In order to solve these inconsistencies, the La-Co-O system was critically reviewed and remodeled focusing especially on phase equilibria. In the present work, thermodynamic database of La-Co-O was also developed as part of a project for developing a thermodynamic database of La-Sr-Co-Fe-O. In our modeling, the $LaCoO_3$ phase was originally modeled as, considering low charge disproportionation (little or no Co^{3+} participates in the $2Co^{3+} \rightarrow Co^{2+} + Co^{4+}$ reaction at low temperature). Later, high charge disproportionation (large amount of Co^{3+}

220

J. Phase Equilib. Diffus. (2019) 40:219–234

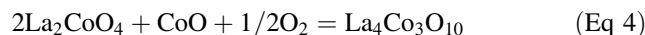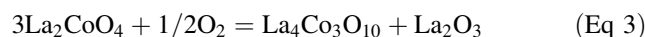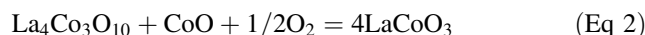participates in the $2Co^{3+} \rightarrow Co^{2+} + Co^{4+}$ reaction) was also tested in the modeling. Two sets of parameters with different cation distribution schemes were thus obtained. Both sets of the parameters can describe phase equilibria and thermodynamic data reasonably well. In addition, attention was given to cation distribution and defect chemistry of the $LaCoO_{3-\delta}$ perovskite phase and a good agreement between experimental data and our model-predicted results was achieved.

2 Literature Review

2.1 Phase Equilibria and Invariant Reactions

La-Co-O was studied first by Sis et al.[4] They investigated valence state, crystallographic and electronic structure of $LaCoO_3$ in reducing atmosphere using thermogravimetry (TG), calorimetry, x-ray diffraction (XRD) and magnetic measurements. They observed that reduction of $LaCoO_3$ proceeds through formation of a series of oxygen-deficient compounds. Janecek and Wirtz[5] investigated the La-Co-O system at 1403 K using XRD. In addition to previously described La_2CoO_4 and $LaCoO_{3-\delta}$, these authors reported another equilibrium compound, $La_4Co_3O_{10}$ to be present in an isothermal section of 1403 K, together with six invariant reactions. $La_4Co_3O_{10}$ is stable at $T > 1600$ K in air.[12] It can also be obtained at lower temperature but with decreased PO_2. Nakamura et al.[6] studied the stability of $LaCoO_3$ and La_2CoO_4 at 1273 K in a PO_2-controlled atmosphere using TG. They determined the Gibbs energy change at 1273 K for the reactions: $LaCoO_3$ (s) = $1/2La_2CoO_4$ (s) + $1/2CoO$ (s) + $1/4O_2$ (gas, 1 bar) and La_2CoO_4 (s) = La_2O_3 (s) + Co (s) + $1/2O_2$ (gas, 1 bar) as 42.7 and 162.0 kJ/mol, respectively. The first reaction was however incorrect, as $LaCoO_3$ will first decompose into $La_4Co_3O_{10}$ with decreasing oxygen partial pressure. Seppänen et al.[7] investigated the stability of $La_4Co_3O_{10}$, La_2CoO_4 and $LaCoO_3$ in a temperature range of 1175-1325 K by means of electromotive force (EMF) measurements and presented an isothermal stability diagram at 1273 K. The Gibbs energy of formation for these three compounds was then evaluated based on their own EMF data and the Gibbs energy functions of La and Co oxides from the literature. Petrov et al.[8,14] studied phase equilibria in La-Co-O as a part of their study on Ln-M-O systems (Ln = La, Pr, Nd; M = Co, Ni, Cu) in a temperature range of 937-1573 K and an oxygen partial pressure range of 10^{-15} to 1 atm. The phase stability was determined by EMF measurements. Based on these data, they calculated Gibbs energy of "potential-forming" reactions and presented several isothermal PO_2-composition phase diagrams. Kitayama[9,10] investigated phase equilibria in La-Co-O at

1473, 1423 and 1373 K in an oxygen partial pressure range of 10^{-12} to 1 atm. The standard Gibbs energy change for a number of reactions was determined using TG measurements. Based on the literature data, the following five invariant reactions exist in the La-Co-O system:

$$2La_4Co_3O_{10} + 1/2O_2 = 6LaCoO_3 + La_2O_3 \qquad \text{(Eq 1)}$$

$$La_4Co_3O_{10} + CoO + 1/2O_2 = 4LaCoO_3 \qquad \text{(Eq 2)}$$

$$3La_2CoO_4 + 1/2O_2 = La_4Co_3O_{10} + La_2O_3 \qquad \text{(Eq 3)}$$

$$2La_2CoO_4 + CoO + 1/2O_2 = La_4Co_3O_{10} \qquad \text{(Eq 4)}$$

$$La_2O_3 + Co + 1/2O_2 = La_2CoO_4 \qquad \text{(Eq 5)}$$

2.2 Characterization of Solid Oxides

In the present work the focus was put on oxide phases. Experimental information on the gas phase and the metallic phases will therefore not be discussed here. The following oxides exist in the La-Co-O system: La_2O_3 (hexagonal, partially ordered hexagonal, cubic), CoO, Co_3O_4, $La_4Co_3O_{10}$, La_2CoO_4 and $LaCoO_{3-\delta}$. Details on the boundary oxides can be found in previous modeling work.[15,16] For the modeling of the ternary extension, structural, chemical, thermochemical properties of the three stable oxides $La_4Co_3O_{10}$, La_2CoO_4 and $LaCoO_{3-\delta}$ are assessed.

$La_4Co_3O_{10}$ was first reported by Janecek and Wirtz,[17] and was later investigated also by other groups.[18,19] It is a Ruddlesden–Popper-type phase with an orthorhombic structure. Parida et al.[1] determined the standard molar Gibbs energy of formation of $La_4Co_3O_{10}$ at 1002-1204 K through EMF measurements.

La_2CoO_4 is orthorhombically distorted relative to the tetragonal K_2NiF_4-type structure.[20] Lewandowski et al.[21] reported that La_2CoO_4 does not exist at the stoichiometric composition. Instead, they proposed a lanthanum-deficient composition, $La_{1.83}CoO_4$. This was however denied by other groups.[8-10] Sreedharan and Pankajavalli[22] determined the Gibbs energy of reaction for La_2O_3 (s) + Co (s) + $1/2O_2$ (gas, 1 bar) = La_2CoO_4 (s) via EMF measurements on a galvanic cell of Pt, La_2CoO_4, La_2O_3, Co/YSZ/O$_2$. They further derived the Gibbs energy of formation of La_2CoO_4 from oxides (La_2O_3 and CoO) in a temperature range of 973-1375 K. Parida et al.[1] determined thermodynamic properties of La_2CoO_4 at 1002-1204 K, also via EMF measurements on a galvanic cell of Pt, La_2CoO_4, La_2O_3, $La_4Co_3O_{10}$/CSZ/Ni, NiO/Pt.

The $LaCoO_{3-\delta}$ perovskite phase has a cubic structure at $T > 1610$ K and a rhombohedral structure at $T < 1610$ K.[12, 23] The cubic-rhombohedral transformation is of second order, as determined by TG–DTA (differential thermal analysis) and XRD measurements.[23] At low oxygen partial pressure, oxygen vacancies form,

J. Phase Equilib. Diffus. (2019) 40:219–234

221

resulting in a further distortion of the perovskite structure to orthorhombic.

The thermodynamic properties of $LaCoO_{3-\delta}$ have been well investigated.[6,8,24–28] Sreedharan and Chandrasekharaiah[24] determined the Gibbs energy of formation and phase transformation of $LaCoO_3$ between 1100 and 1325 K via EMF measurements. They used two types of galvanic cells: Pt/Ni, NiO/CSZ/Co, La_2O_3, $LaCoO_3$/Pt and Pt/Ni, NiO/CSZ/CoO, La_2O_3, $LaCoO_3$/Pt. However, both cells did not reach equilibrium and therefore their derived phase relations were wrong.[6,8,25] Stølen et al.[26] and Horinouch et al.[28] measured the heat capacity of $LaCoO_3$ from 13 to 1000 K and 80-950 K by adiabatic calorimetry, respectively. Parida et al.[1] determined the standard molar Gibbs energy of formation for $LaCoO_3$ at 1002-1204 K via EMF measurements. They chose same galvanic cell configuration as Sreedharan and Chandrasekharaiah[24] and reported that the Gibbs energy of formation for $LaCoO_3$ is higher than the value reported by Nakamura et al. from[6] and Kitayama.[10] Cheng et al.[27] determined the enthalpy of formation for $LaCoO_3$ from constituent oxides at 298 K as -107.64 ± 1.77 kJ/mol by high-temperature oxide melt solution calorimetry.

Oxygen deficiency in $LaCoO_{3-\delta}$ was measured by a number of groups.[29–32] Seppänen et al.[29] determined oxygen deficiency in $LaCoO_{3-\delta}$ as a function of oxygen partial pressure at temperatures between 1178 and 1311 K using the coulometric titration method. They measured oxygen deficiency of $LaCoO_{3-\delta}$ in equilibrium with either La_2O_3 or CoO at 1200, 1255 and 1288 K and derived partial molar enthalpy and entropy of oxygen in $LaCoO_{3-\delta}$. Mizusaki et al.[30] used TG to determine oxygen nonstoichiometry in $LaCoO_{3-\delta}$ at 1123, 1173, 1223 and 1273 K and $PO_2 = 10^{-5} - 1$ atm. Petrov et al.[31] studied oxygen nonstoichiometry of $LaCoO_{3-\delta}$ at 1273-1773 K as a function of PO_2 using TG. Recently, Zuev et al.[32] measured oxygen nonstoichiometry of lanthanum cobaltite as a function of oxygen partial pressure at $1173 - 1323$ K by coulometric titration. Their results were also in agreement with those from Seppänen et al.[29]

Beside thermodynamic properties and oxygen nonstoichiometry, the electronic structure of $LaCoO_{3-\delta}$ has drawn special interest, as it influences magnetic properties, electronic conductivity and thermal conductivity. Goodenough[33] investigated the transition in $LaCoO_{3-\delta}$ from localized electron to collective electron by XRD, DTA and TG measurements and constructed a model for cobalt cation configuration in $LaCoO_{3-\delta}$ at various temperature intervals. It was found that Co^{2+} (high spin) and Co^{4+} (low spin) formed only at $T > 673$ K, and there is a first order transition at 1210 K from localized electron to collective electron. Bhide[34] et al. investigated this transition but using Mössbauer spectroscopy. They concluded that Co^{2+}

(low spin) and Co^{4+} (high spin) already formed at $T > 200$ K and Co^{3+} disappeared completely at 1210 K. Abbate et al.[35] re-determined electronic structure of $LaCoO_{3-\delta}$ and found no evidence of charge disproportionation at a temperature range of 80-630 K. The electronic structure and spin state of $LaCoO_{3-\delta}$ were recently studied by groups of authors.[36–39] Despite tremendous interests and intensive research activities over the past decades, the electronic structure of $LaCoO_{3-\delta}$ and the conduction mechanism are still topics of controversial discussions.

3 Thermodynamic Modeling

Several efforts have been carried out on thermodynamic modeling of the La-Co-O system. Yokokawa et al.[40] modeled the thermodynamic properties of the three oxides ($LaCoO_3$, La_2CoO_4 and $La_4Co_3O_{10}$) in order to construct a chemical potential diagram for La-Co-O. All these oxides were treated as stoichiometric compounds, and no defects were considered. Yang et al.[12] and Saal[13] modeled La-Co-O using the CALPHAD methodology. Their set of parameters provides a good agreement with experimentally measured oxygen non-stoichiometry data. However, the phase diagrams calculated using their databases are in contradiction with experimental findings with regard to stability of the $LaCoO_{3-\delta}$ perovskite phase. In our assessment we thus put a big effort to obtain both correct phase boundaries as well as reliable descriptions of the defect chemistry and cation disproportionation of the lanthanum cobaltite.

To benefit from the existing databases of La_2O_3-SrO[41] and La-Fe-O[42] and to allow for an efficient extrapolation to the thermodynamic database of La-Sr-Co-Fe-O, in the current work, the thermodynamic description of the three sub-systems in La-Co-O were taken directly from literature[15,16,43] with minor modification: La-O by Grundy et al.,[15] Co-O by Chen et al.,[16] and La-Co by Wang et al.[43] The latest experimental data on the phase transition/fusion temperature and enthalpy of La_2O_3 by Ushakov et al.[44] were thus not employed to remodel the La-O system. However, a comparison of these data is included here and presented as Table 1. Between the experimentally measured values reported by Ushakov et al.[44] and the calculated values reported by Grundy et al.[15] and Zinkevich,[45] the main difference lies in the transition enthalpies for La_2O_3. Further investigations are hence necessary to resolve the inconsistency. The parameters for the ternary La-Co-O system were optimized using the experimental data as described in section 2. The Compound Energy Formalism (CEF),[46] which is widely used in CALPHAD assessments, was employed to describe Gibbs energy for

222

J. Phase Equilib. Diffus. (2019) 40:219–234

Table 1 Temperature and enthalpy of phase transition/fusion for La$_2$O$_3$ reported in the literature

A-H		H-X		X-liquid		References
ΔH, kJ/mol	T, K	ΔH, kJ/mol	T, K	ΔH, kJ/mol	T, K	
46	2313	60	2383	75	2586	15
23 ± 5	2319±5	17±5	2387±5	78±10	2574 ± 10	44
32.35	2313	10.84	2373	98.14	2578	45

all the phases in La-Co-O. The lattice stability for pure elements was adopted from Dinsdale.[47] The magnetic contribution to the Gibbs energy was modeled using the "Hillert–Jarl–Inden" model proposed by Inden[48] and further modified by Hillert and Jarl.[49]

3.1 Liquid

In the present work, the liquid phase was treated as an ideal extrapolation of the liquid from the subsystems La-O[15] and Co-O,[16] where the liquid phase was modeled all using the ionic two-sublattice model.[50,51] This model was developed within the framework of CEF, with one sublattice containing charged cations and the other containing charged anions and vacancies. The liquid phase in La-Co-O is described as:

$$\left(Co^{2+}, Co^{3+}, La^{3+}\right)_p \left(O^{2-}, Va^{q-}\right)_q$$
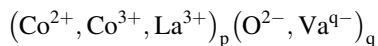
where

$$p = 2y_O^{2-} + qy_{Va} \tag{Eq 6}$$

$$q = 2y_{Co}^{2+} + 3y_{Co}^{3+} + 3y_{La}^{3+} \tag{Eq 7}$$

The Gibbs energy of the liquid phase is expressed as:

$$G_m^L = q \sum_i y_i y_{Va}\,^0 G_{i:Va}^L + \sum_i y_i y_{O^{2-}}\,^0 G_{i:O^{2-}}^L$$
$$+ pRT \sum_i y_i \ln y_i + qRT \sum_j y_j \ln y_j + {}^E G_m^L \tag{Eq 8}$$

where i represents the constituents in the first sublattice, and j represents the constituents in the second sublattice. y_i denotes the site-fraction of i in the first sublattice. The excess Gibbs energy ${}^E G_m^L$ is formulated as the following:

$${}^E G_m^L = \sum_{i_m} \sum_{i_n \neq i_m} y_{i_m} y_{i_n} \left(y_{O^{2-}} L_{i_m, i_n : O^{2-}}^L + q y_{Va}^3 L_{i_m, i_n : Va}^L\right)$$
$$+ \sum_{i_m} y_{i_m} y_{O^{2-}} y_{Va} L_{i_m : O^{2-}, Va}^L \tag{Eq 9}$$

where i_m and i_n represents the constituents in the first sublattice. In the above expressions, colons were used to separate species on different sublattices and commas to separate species on the same sublattice. In the present work, no ternary (La-Co-O) parameter was optimized for

the liquid phase due to lack of experimental data. The calculated liquidus shall therefore be treated with caution.

3.2 Metallic Phases

In the present work, the thermodynamic descriptions for the metallic phases were taken from binary sub-systems[15,16,43] with ideal extrapolation. No ternary or quaternary parameter was used. Oxygen solubility in pure metal (BCC, FCC, HCP and DHCP) was modeled using the two-sublattice model with metal atoms on the first sublattice and oxygen and vacancies on the second sublattice. In La-Co-O, the models read as the following:

BCC : $(La, Co)_1 (O, Va)_3$
FCC : $(La, Co)_1 (O, Va)_1$
HCP : $(Co)_1 (O, Va)_{0.5}$
DHCP : $(La)_1 (O, Va)_{0.5}$
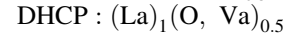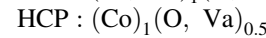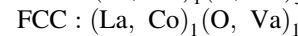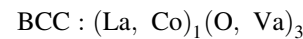
The binary parameters were taken from literatures,[15,16,43] except for the BCC phase. In Co-O, the BCC phase was modeled using the model $(Co)_1 (O, Va)_3$, while in La-O the BCC-La was modeled as $(La)_1 (O, Va)_{1.5}$. In the present work, the BCC-La phase was remodeled as $(La)_1 (O, Va)_3$ in accordance with the BCC-Co phase. The thermodynamic descriptions of the inter-metallic compounds in La-Co were taken from literature.[43]

3.3 Oxides in the Boundary Systems

The Gibbs energy functions for CoO and Co$_3$O$_4$ were taken from Chen et al.[16] For La-O, Grundy et al.[15] modeled the polymorphic-La$_2$O$_3$ as nonstoichiometric. In their calculated phase diagram of La-O, solid La$_2$O$_3$ appears too stable when interacting with the liquid phase. Later, they revised the thermodynamic description of the solid La$_2$O$_3$ phases where the deviation from stochiometry was ignored.[41] It was shown that the calculated melting temperature of La$_2$O$_3$ fits better with the experimental results. Zinkevich et al.[52] also modeled the La-O system, but their assessment was based on a limited amount of experimental data. In the present work, we adopted the revised thermodynamic descriptions for La$_2$O$_3$ from Grundy et al.[41]

No mutual solubility was found between La oxides and Co oxides and was therefore not considered in the present work.

3.4 $La_4Co_3O_{10}$ and La_2CoO_4

In the present work, $La_4Co_3O_{10}$ and La_2CoO_4 were treated also as stoichiometric compound. The Gibbs energy functions were taken from Yokokawa et al.,[40] which were adopted by the SGTE SSUB database.[53] The Gibbs energy function for $La_4Co_3O_{10}$ was further adjusted in the present work in order to reproduce recently reported thermodynamic data and phase diagram data.[7–10]

3.5 Perovskite ($LaCoO_{3-\delta}$)

We modeled the perovskite phase as one single phase without differentiating the cubic distortion structures (orthorhombic, and rhombohedral). A 3-sublattice model was used, with the first sublattice (A site) for La cations and vacancies, the second sublattice (B site) for Co cations and vacancies, and the third sublattice (O site) for oxide ions and oxygen vacancies. For La-Co-O, beside Co^{3+}, Co^{2+} and Co^{4+} were also introduced into the B site in order to model charge disproportionation ($2Co^{3+} \rightarrow Co^{2+}+Co^{4+}$). Cation vacancies were introduced into the A and B sites and oxygen vacancies to the O site, respectively, to model the perovskite nonstoichiometry, and the model reads $(La^{3+},Va)_1(Co^{2+},Co^{3+}, Co^{4+},Va)_1 (O^{2-}, Va)_3$.

The Gibbs energy function of the perovskite phase (the non-magnetic part) is given by the following expression:

$$G_m^{perovskite} = \sum_i \sum_j \sum_k y_i y_j y_k {}^oG_{i:j:k}^{perovskite} + RT \sum_i y_i \ln y_i$$
$$+ RT \sum_j y_j \ln y_j + 3RT \sum_k y_k \ln y_k$$
$$+ {}^EG_m^{perovskite}$$

(Eq 10)

where i, j, k represent the constituents in the first, second and third sublattice, respectively. y_i denotes the site-fraction of i in the first sublattice. ${}^oG_{i:j:k}^{perovskite}$ is the Gibbs energy of the end-member component $(i)_1(j)_1(k)_3$.

According to the current model, 16 end-members (${}^oG_{i:j:k}^{perovskite}$ terms) need to be assigned with a Gibbs energy term. Most of these end-members have a net charge and therefore do not physically exist. The strategy to obtain the Gibbs energy terms for these end-members is to choose appropriate neutral end-members or their combinations as model parameters, which can be optimized with experimental data. Similar to previous modeling of the perovskite phase,[42,54,55] a number of the most important end-members or their combinations were chosen as model parameters and were listed below:

Stoichiometric $LaCoO_3$: $(La^{3+})_1(Co^{3+})_1(O^{2-})_3$. Its Gibbs energy function is given by:

$${}^oG_{La^{3+}:Co^{3+}:O^{2-}}^{perovskite} = GL3CO$$

(Eq 11)

where GL3CO was remodeled based on the Gibbs energy functions from Yokokawa et al.[40] with consideration of new enthalpy of formation[27] and heat capacity data.[26,28]

Reduced $LaCoO_3$: $(La^{3+})_1(Co^{2+})_1(O_{5/6}^{2-}, Va_{1/6})_3$. Its Gibbs energy function is given by:

$$G_m = \frac{5}{6} {}^oG_{La^{3+}:Co^{2+}:O^{2-}}^{perovskite} + \frac{1}{6} {}^oG_{La^{3+}:Co^{2+}:Va}^{perovskite}$$
$$+ 3RT\left(\frac{5}{6}\ln\frac{5}{6} + \frac{1}{6}\ln\frac{1}{6}\right)$$
$$= \frac{1}{2} {}^oG^{La_2O_3} + {}^oG^{CoO} + A_1 + B_1 * T$$

(Eq 12)

where ${}^oG^{La_2O_3}$ and ${}^oG^{CoO}$ represent the Gibbs energy functions of stoichiometric A-La_2O_3 and CoO respectively and were taken from Grundy et al.[41] and Chen et al.[16] A_1 and B_1 are the parameters to be optimized in the present work.

Oxidized Co rich $LaCoO_3$ $(La_{2/3}^{3+}, Va_{1/3})_1(Co^{4+})_1(O^{2-})_3$

$$G_m = \frac{2}{3} {}^oG_{La^{3+}:Co^{4+}:O^{2-}}^{perovskite} + \frac{1}{3} {}^oG_{Va:Co^{4+}:O^{2-}}^{perovskite}$$
$$+ RT\left(\frac{2}{3}\ln\frac{2}{3} + \frac{1}{3}\ln\frac{1}{3}\right)$$
$$= \frac{1}{3} {}^oG^{La_2O_3} + {}^oG^{CoO} + \frac{1}{2} {}^oG^{O_2} + A_2 + B_2 * T$$

(Eq 13)

Oxidized Co deficient $LaCoO_3$ $(La^{3+})_1(Co_{3/4}^{4+}, Va_{1/4})_1(O^{2-})_3$.

$$G_m = \frac{3}{4} {}^oG_{La^{3+}:Co^{4+}:O^{2-}}^{perovskite} + \frac{1}{4} {}^oG_{La^{3+}:Va:O^{2-}}^{perovskite}$$
$$+ RT\left(\frac{3}{4}\ln\frac{3}{4} + \frac{1}{4}\ln\frac{1}{4}\right)$$
$$= \frac{1}{2} {}^oG^{La_2O_3} + \frac{3}{4} {}^oG^{CoO} + \frac{3}{8} {}^oG^{O_2} + A_3 + B_3 * T$$

(Eq 14)

where ${}^oG^{O_2}$ was from Dinsdale[47] and A_2, A_3, B_2, and B_3 are the parameters to be optimized in the present work.

To be consistent with the thermodynamic descriptions of the perovskite phase in La-Mn-O[54] (and in La-Fe-O[42]), the Gibbs energy terms for the following four end-members ${}^oG_{La^{3+}:Va:O^{2-}}^{perovskite}$, ${}^oG_{Va:Va:O^{2-}}^{perovskite}$, ${}^oG_{La^{3+}:Va:Va}^{perovskite}$, ${}^oG_{Va:Va:Va}^{perovskite}$ were taken from Grundy et al.,[54] which are common for all the three systems.

All the other end-members are correlated by the following reciprocal relations:

$${}^oG_{La^{3+}:Co^{3+}:O^{2-}}^{perovskite} + {}^oG_{Va:Co^{3+}:Va}^{perovskite} - {}^oG_{La^{3+}:Co^{3+}:Va}^{perovskite} - {}^oG_{Va:Co^{3+}:O^{2-}}^{perovskite} = \Delta G_1$$

(Eq 15)

224

J. Phase Equilib. Diffus. (2019) 40:219–234

$${}^{o}G_{La^{3+}:Co^{3+}:O^{2-}}^{perovskite} + {}^{o}G_{La^{3+}:Co^{4+}:Va}^{perovskite} - {}^{o}G_{La^{3+}:Co^{4+}:O^{2-}}^{perovskite} - {}^{o}G_{La^{3+}:Co^{3+}:Va}^{perovskite} = \Delta G_2$$

(Eq 16)

$${}^{o}G_{La^{3+}:Co^{2+}:O^{2-}}^{perovskite} + {}^{o}G_{Va:Co^{3+}:O^{2-}}^{perovskite} - {}^{o}G_{La^{3+}:Co^{3+}:O^{2-}}^{perovskite} - {}^{o}G_{Va:Co^{2+}:O^{2-}}^{perovskite} = \Delta G_3$$

(Eq 17)

$${}^{o}G_{La^{3+}:Co^{3+}:O^{2-}}^{perovskite} + {}^{o}G_{Va:Co^{4+}:O^{2-}}^{perovskite} - {}^{o}G_{La^{3+}:Co^{4+}:O^{2-}}^{perovskite} - {}^{o}G_{Va:Co^{3+}:O^{2-}}^{perovskite} = \Delta G_4$$

(Eq 18)

$${}^{o}G_{Va:Co^{3+}:O^{2-}}^{perovskite} + {}^{o}G_{Va:Co^{2+}:Va}^{perovskite} - {}^{o}G_{Va:Co^{2+}:O^{2-}}^{perovskite} - {}^{o}G_{Va:Co^{3+}:Va}^{perovskite} = \Delta G_5$$

(Eq 19)

$${}^{o}G_{La^{3+}:Co^{2+}:Va}^{perovskite} + {}^{o}G_{Va:Co^{3+}:Va}^{perovskite} - {}^{o}G_{La^{3+}:Co^{3+}:Va}^{perovskite} - {}^{o}G_{Va:Co^{2+}:Va}^{perovskite} = \Delta G_6$$

(Eq 20)

$${}^{o}G_{La^{3+}:Co^{3+}:Va}^{perovskite} + {}^{o}G_{Va:Co^{4+}:Va}^{perovskite} - {}^{o}G_{La^{3+}:Co^{4+}:Va}^{perovskite} - {}^{o}G_{Va:Co^{3+}:Va}^{perovskite} = \Delta G_7$$

(Eq 21)

$${}^{o}G_{La^{3+}:Co^{2+}:O^{2-}}^{perovskite} + {}^{o}G_{La^{3+}:Co^{3+}:Va}^{perovskite} - {}^{o}G_{La^{3+}:Co^{3+}:O^{2-}}^{perovskite} - {}^{o}G_{La^{3+}:Co^{2+}:Va}^{perovskite} = \Delta G_8$$

(Eq 22)

In this work, the reciprocal energy $\Delta G_x = 0$ ($x = 1-8$) was chosen.[56] The Gibbs energy functions for the 12 end-members can be derived by solving Eq 11 to 22.

The excess Gibbs energy ${}^{E}G_m^{perovskite}$ is formulated as the following:

$$
\begin{aligned}
{}^{E}G_m^{perovskite} = & \sum_{i_l}\sum_{i_k \neq i_l}\sum_{j_m} y_{i_k}y_{i_l}y_{j_m}L_{i_k,i_l:j_m:O^{2-}}^{perovskite} \\
& + \sum_{i_l}\sum_{j_m}\sum_{j_n \neq j_m} y_{i_l}y_{j_m}y_{j_n}L_{i_l:j_m,j_n:O^{2-}}^{perovskite}
\end{aligned}
$$

(Eq 23)

where i_k, i_l represents the constituents in the first sublattice (A site), and j_m, j_n represents the constituents in the second sublattice (B site).

3.6 Optimization

Table 2 lists two sets of optimized thermodynamic parameters obtained in the present work for the three oxide phases in La-Co-O. Due to small modifications on the thermodynamic descriptions of the BCC-La and La$_2$O$_3$ phases in the current work, the La-O phase diagram was re-calculated and it agrees reasonably well with the ones published by Grundy et al.[15] and Povoden-Karadeniz et al.[42] During the optimization, all experimental data were carefully assessed. The evaluation of the model parameters was obtained by recurrent runs of the PARROT program[57] in the Thermo-Calc software, which works by minimizing the square sum of the differences between experimental values and computed ones. In the optimization, each piece of experimental information is given with certain weight. The weights were adjusted during the assessment until most of the experimental data were accounted for within the claimed uncertainty limits.

The optimization of model parameters of stoichiometric phases is straight-forward. As mentioned in section 3.4, the parameter for La$_4$Co$_3$O$_{10}$ was further optimized using the thermodynamic and phase diagram data. On the other hand, the perovskite phase is much more interesting and demanding. GL3CO in Eq 11 were optimized using relevant thermodynamic and phase diagram data. The magnetic parameters Tc and b were fitted to the Cp data around the magnetic transition temperature. In order to take into account the magnetic transition at around 530 K and the charge disproportion at high temperature, three temperature intervals were used for GL3CO. A_1 and B_1 in Eq 12 control charge disproportionation and were optimized using oxygen nonstoichiometry data. In addition, A_2 and B_2 in Eq 13 and A_3 together with B_3 in Eq 14 were optimized in order to achieve a satisfying agreement with the oxygen non-stoichiometry data. Two sets of parameters were obtained in the end: *Parameter Set A* is suggested for low charge disproportionation (nearly 0% at $T < 700$ K) and *Parameter Set B* is for high charge disproportionation (100% at low temperature). LaCoO$_{3-\delta}$ shows very narrow composition range with respect to the La/Co ratio. To prevent any deviation from a La/Co ratio of 1 in the calculated phase diagrams, two interaction parameters ${}^{0}L_{La^{3+},Va:Co^{4+}:O^{2-}}^{perovskite}$ and ${}^{0}L_{La^{3+}:Co^{4+},Va:O^{2-}}^{perovskite}$ were assigned with a value of 1,000,000 in *Parameter Set B*.

4 Results and Discussion

In the present work, two sets of thermodynamic parameters were obtained representing different charge disproportionation schemes in LaCoO$_{3-\delta}$. Figure 1 plots calculated site fractions in LaCoO$_{3-\delta}$ in air using these two sets of parameters. With *Parameter Set A*, LaCoO$_{3-\delta}$ shows no charge disproportionation at low temperature. Co^{2+} and Co^{4+} start forming at about 700 K, which is in agreement with Goodenough and Abbate et al.[33,35] With *Parameter Set B*, LaCoO$_{3-\delta}$ shows high charge disproportionation, with Co^{2+} and Co^{4+} forming at all temperatures. Regarding thermodynamic properties and phase diagrams, both sets of the parameters represent experimental data equally well. The comparison between our calculated results and the experimental data in the following is carried out mainly for *Parameter Set A* to save space.

4.1 Thermodynamic Properties

In the present work, the Gibbs energy functions of La$_2$CoO$_4$ and La$_4$Co$_3$O$_{10}$ were based on those from Yokokawa et al.[40] with minor change, and the comparison of the

Table 2 Models and parameters for the ternary oxide phases in La-Co-O system

Phase	Model/parameters	References
$La_4Co_3O_{10}$	$(La_4Co_3O_{10})$	
	$^oG^{La_4Co_3O_{10}} - 4H_{La}^{SER} - 3H_{Co}^{SER} - 10H_O^{SER} = GLA4CO3O10$	This work
La_2CoO_4	$(La^{3+})_2\,(Co^{2+})_1(O^{2-})_4$	
	$^oG^{La_2CoO_4}_{La^{3+}:Co^{2+}:O^{2-}} - 2H_{La}^{SER} - H_{Co}^{SER} - 4H_O^{SER} = GLA2COO4$	40
Perovskite	$(La^{3+}, Va)(Co^{2+},Co^{3+},Co^{4+}, Va)_1(O^{2-}, Va)_4$	
		This work
	$^oG^{perovskite}_{La^{3+}:Co^{2+}:O^{2-}} - H_{La}^{SER} - H_{Co}^{SER} - 3H_O^{SER} = +GLC2OV + 0.5GHSEROO + 11.2379T$	
	$^oG^{perovskite}_{Va:Co^{2+}:O^{2-}} - H_{Co}^{SER} - 3H_O^{SER} = +0.5GVVV + GLC2OV - 2GL4VO + 1.5GLV4O$ $+ 2GHSEROO + 11.2379T$	This work
	$^oG^{perovskite}_{La^{3+}:Co^{3+}:O^{2-}} - H_{La}^{SER} - H_{Co}^{SER} - 3H_O^{SER} = +GL3CO$	This work
	$^oG^{perovskite}_{Va:Co^{3+}:O^{2-}} - H_{Co}^{SER} - 3H_O^{SER} = +GL3CO + 0.5GVVV - 2GL4VO + 1.5GLV4O$ $+ 1.5GHSEROO - 1.41254T$	This work
	$^oG^{perovskite}_{La^{3+}:Co^{4+}:O^{2-}} - H_{La}^{SER} - H_{Co}^{SER} - 3H_O^{SER} = +^1/_6GVVV + ^2/_3GL4VO + 0.5GLV4O$ $- 0.5GHSEROO + 5.76283T$	This work
	$^oG^{perovskite}_{Va:Co^{4+}:O^{2-}} - H_{Co}^{SER} - 3H_O^{SER} = +^1/_3GVVV - ^4/_3GL4VO + 2GLV4O$ $+ GHSEROO + 4.35029T$	This work
	$^oG^{perovskite}_{La^{3+}:Va:O^{2-}} - H_{La}^{SER} - 3H_O^{SER} = +2GL4O - 1.5GV4O + 0.5GVVV$ $+ 1.5GHSEROO + 1.41263T$	54
	$^oG^{perovskite}_{Va:Va:O^{2-}} - 3H_O^{SER} = +GVVV + 3GHSEROO$	54
	$^oG^{perovskite}_{La^{3+}:Co^{2+}:Va} - H_{La}^{SER} - H_{Co}^{SER} = +GLC2OV - 2.5GHSEROO + 11.2379T$	This work
	$^oG^{perovskite}_{Va:Co^{2+}:Va} - H_{Co}^{SER} = +0.5GVVV + GLC2OV - 2GL4VO + 1.5GLV4O$ $- GHSEROO + 9.82536T$	This work
	$^oG^{perovskite}_{La^{3+}:Co^{3+}:Va} - H_{La}^{SER} - H_{Co}^{SER} = +GL3CO - 3GHSEROO$	This work
	$^oG^{perovskite}_{Va:Co^{3+}:Va} - H_{Co}^{SER} = +GL3CO + 0.5GVVV - 2GL4VO + 1.5GLV4O$ $- 1.5GHSEROO - 1.41254T$	This work
	$^oG^{perovskite}_{La^{3+}:Co^{4+}:Va} - H_{La}^{SER} - H_{Co}^{SER} = -^1/_6GVVV + ^2/_3GL4VO + 0.5GLV4O$ $- 3.5GHSEROO + 5.76283T$	This work
	$^oG^{perovskite}_{Va:Co^{4+}:Va} - H_{Co}^{SER} = +^1/_3GVVV - ^4/_3GL4VO + 2GLV4O$ $- 2GHSEROO + 4.35029T$	This work
	$^oG^{perovskite}_{La^{3+}:Va:Va} - H_{La}^{SER} = +2GL4O + 0.5GVVV - 1.5GV4O$ $- 1.5GHSEROO + 1.41263T$	54
	$^oG^{perovskite}_{Va:Va:Va} = GVVV$	54

Interaction parameters and functions	

Parameter set A

$GLA4CO3O10 = -4672982.57 + 2320.29T - 402T\ln(T) - 0.02715T^2 + 2566000T^{-1}$	This work
$GLA2COO4 = -2095975.55 + 951.68T - 167.49T\ln(T) - 0.010645T^2 + 938000T^{-1}$	40
$GLC2OV = 0.5GLA2O3D + GCOOS + 45388.14 - 14.77T$	This work
$GL4VO = 0.5GLA2O3D + 0.75GCOOS + 0.75GHSEROO - 68796.23 - 28.21T$	This work
$GLV4O = ^1/_3GLA2O3D + GCOOS + GHSEROO - 85014.24 + 223.25T$	This work
$GL3CO = -1256078 - 82.59T + 6.17T\ln(T) - 0.14132T^2 - 1179500T^{-1}\,298.15 < T < 530K$ $- 1301031 + 736.07T - 126.863T\ln(T) - 0.0052865T^2 - 2193227T^{-1}\,530 < T < 1000$ $- 1296189 + 679.47T - 115.1T\ln(T) - 0.009245T^2 + 958500T^{-1}\,1000 < T < 3000$	This work

226

J. Phase Equilib. Diffus. (2019) 40:219–234

Table 2 continued

Interaction parameters and functions	
$GVVV = 6GL2O + 4GL4O + 3GV4O - 12GL3O - 254212$	54
$p = 0.28$ $T_c^{perovskite} = 530y_{i:j:k}$ $\beta^{perovskite} = 0.08221y_{i:j:k}$	This work
$i = La^{3+}$ $j = Co^{2+}, Co^{3+}, Co^{4+}$ $k = O^{2-}, Va$	
Parameter set B	
${}^0L_{La^{3+},Va:Co^{4+}:O^{2-}}^{perovskite} = +1,000,000$	This work
${}^0L_{La^{3+}:Co^{4+},Va:O^{2-}}^{perovskite} = +1,000,000$	This work
$GLA4CO3O10 = -4694982.57 + 2329.49T - 402T\ln(T) - 0.02715T^2 + 2566000T^{-1}$	40
$GLA2COO4 = -2095975.55 + 951.68T - 167.49T\ln(T) - 0.010645T^2 + 938000T^{-1}$	40
$GLC2OV = 0.5GLA2O3D + GCOOS - 21830.3 + 22.37T$	This work
$GL4VO = 0.5GLA2O3D + 0.75GCOOS + 0.75GHSEROO - 101531.5 - 8.66T$	This work
$GLV4O = {}^1/_3GLA2O3D + GCOOS + GHSEROO - 233150.3 + 316.78T$	This work
$GL3CO = -1261010.71 - 70.3237561T + 6.17T\ln(T) - 0.14132T^2 - 1179500T^{-1}298.15 < T < 530K$	This work
$\qquad - 1301031.07 + 751.034485T - 125.1T\ln(T) - 0.009245T^2 + 958500T^{-1}550 < T < 1000$	
$\qquad - 1288831.07 + 669.968423T - 115.1T\ln(T) - 0.009245T^2 + 958500T^{-1}1000 < T < 3000$	
$GVVV = 6GL2O + 4GL4O + 3GV4O - 12GL3O - 254212$	54
$p = 0.28$ $T_c^{perovskite} = 530y_{i:j:k}$ $\beta^{perovskite} = 0.974y_{i:j:k}$	This work
$i = La^{3+}$ $j = Co^{2+}, Co^{3+}, Co^{4+}$ $k = O^{2-}, Va$	

All parameters are in SI units: J, mol, K and Pa

Fig. 1 Site fractions in $LaCoO_{3-\delta}$ in air. (a) calculated using *Parameter Set A*, (b) calculated using *Parameter Set B*
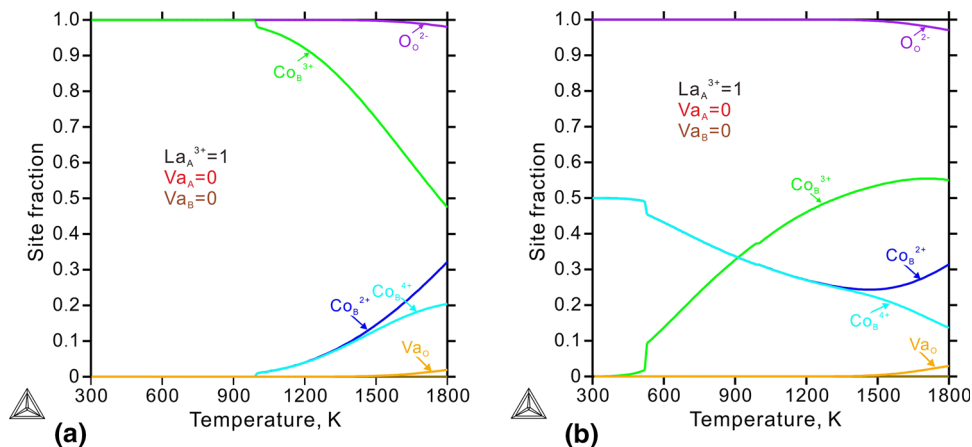

Table 3 Calculated thermodynamic properties of $LaCoO_3$ using parameter Set A in comparison with the experimental data

Thermodynamic data	Temperature, K	Calculated	Experiment	References
$\Delta H_{f,ox}^{\circ}$, kJ/mol	298	− 118.9	− 107.64	27
$\Delta H_{f,el}^{\circ}$, kJ/mol	298	− 1253.5	− 1241.34	27
S, J/mol K	298	112	111	26
S, J/mol K	1000	276	276	26

calculated Gibbs energy of formation with experimental data for these two phases is therefore excluded.

The comparison between the calculated thermodynamic properties and the experimental ones[26,27] is listed in

Table 3. The calculated entropies at 298 and 1000 K were 112 J/(mol K) and 276 J/(mol K), respectively, which agree well with the experimental results.[26] Using Parameter Set A, the enthalpy of formation for $LaCoO_3$ at
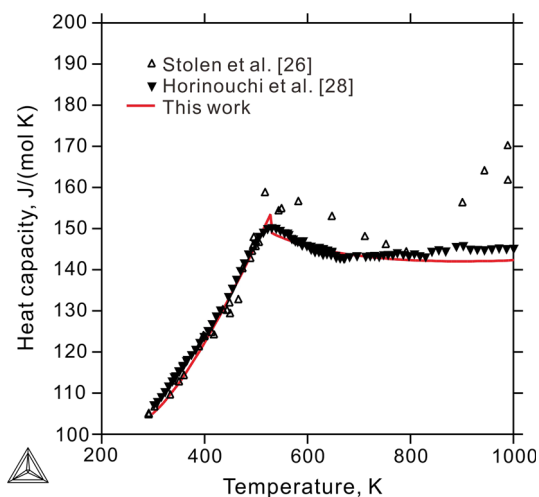
Fig. 2 Calculated heat capacity of LaCoO$_3$ as a function of temperature using *Parameter Set A* in comparison with the experimental results[26,28]
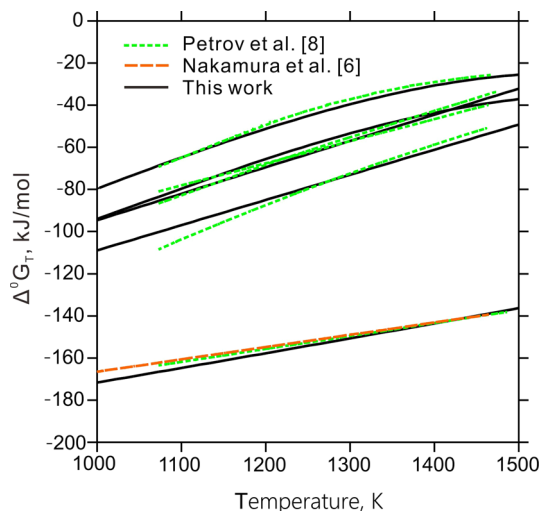

Fig. 3 Calculated Gibbs energy of reaction as a function of temperature using *Parameter Set A* in comparison with the experimental results.[6,8] (a) 2La$_4$Co$_3$O$_{10}$ (s) +1/2O$_2$ (gas, air) = 6LaCoO$_3$ (s) + La$_2$O$_3$ (s); (b) La$_4$Co$_3$O$_{10}$ (s) +CoO (s) +1/2O$_2$ (gas, air) = 4LaCoO$_3$ (s); (c) 3La$_2$CoO$_4$ (s) + 1/2O$_2$ (gas, air) = La$_4$Co$_3$O$_{10}$ (s) + La$_2$O$_3$ (s); (d) 2La$_2$CoO$_4$ (s) + CoO (s) + 1/2O$_2$ (gas, air) = La$_4$Co$_3$O$_{10}$ (s) and (e) La$_2$O$_3$ (s) + Co (s) + 1/2O$_2$ (gas, air) = La$_2$CoO$_4$ (s)

298.15 K was calculated as − 118.9 kJ/mol from oxides (La$_2$O$_3$ and CoO) and − 1253.5 kJ/mol from elements respectively, about 11-12 kJ more negative than the experimentally measured values reported by Cheng et al.[27] (− 107.42 ± 1.77 kJ/mol from oxides and − 1241.34 ± 2.34 kJ/mol from elements). Although our calculated values are a bit outside the uncertainty range estimated based on the experimental values, they are still

considered reasonable since the current thermodynamic description of LaCoO$_3$ can reproduce most of the experimental data well, including heat capacity, Gibbs energy of formation, cation distribution and most importantly the composition of LaCoO$_3$ phase at low temperature as will be shown below. Figure 2 shows the calculated heat capacity of LaCoO$_3$ as a function of temperature using *Parameter Set A* in comparison with the experimental results.[26,28] The calculated results fit the experimental data points well. Figure 3 plots the calculated Gibbs energy of reaction as a function of temperature using *Parameter Set A*. The reactions are (a) 2La$_4$Co$_3$O$_{10}$ (s) + 1/2O$_2$ (gas, air) = 6LaCoO$_3$ (s) + La$_2$O$_3$ (s); (b) La$_4$Co$_3$O$_{10}$ (s) + CoO (s) + 1/2O$_2$ (gas, air) = 4LaCoO$_3$ (s); (c) 3La$_2$CoO$_4$ (s) + 1/2O$_2$ (gas, air) = La$_4$Co$_3$O$_{10}$ (s) + La$_2$O$_3$ (s); (d) 2La$_2$CoO$_4$ (s) + CoO (s) + 1/2O$_2$ (gas, air) = La$_4$Co$_3$O$_{10}$ (s) and (e) La$_2$O$_3$ (s) + Co (s) + 1/2O$_2$ (gas, air) = La$_2$CoO$_4$ (s). A good agreement with the experimental results is achieved.

4.2 Phase Diagrams

Figure 4 presents the calculated La-Co-O phase diagrams in air and Fig. 5 shows the calculated isothermal PO_2-composition phase diagrams at 1373 K, using both sets of parameters. The experimental data from Petrov et al.[14] were included for comparison. The calculated phase diagrams based on the two different sets of parameters agree with the experimental data equally well. Some difference can be found in the calculated temperatures for various invariant reactions in air (Fig. 4) and at $PO_2 = 1$ Pa (Table 4). Further experimental studies on these invariant reactions are recommended in order to further narrow down the uncertainties.

The calculated isothermal PO_2-composition phase diagrams at different temperatures are plotted in Fig. 6. These phase diagrams are all based on *Parameter Set A*. With decreasing temperature, the stability range for the perovskite phase extends to lower oxygen partial pressure. Figure 7 shows the calculated stability phase diagrams using *Parameter Set A*. The calculations were done at different Co contents: $x(Co)/(x(Co) + x(La)) = 0.3$, 0.7 and 0.5. The single phase or two-phase region is labeled with phase names and the line between two neighboring regions represents a three-phase region (univariant). At high Co content (Fig. 7a) the calculation fits the experimental data very well. At low Co content (Fig. 7b), the calculated stability range for La$_4$Co$_3$O$_{10}$ is slightly larger than the experimentally determined one, with respect to both temperature and oxygen partial pressure. For SOFC applications, the La/Co ration of 1 is the most relevant, which is presented in Fig. 7(c). This kind of phase diagram can be used to explore the stability range for the desired
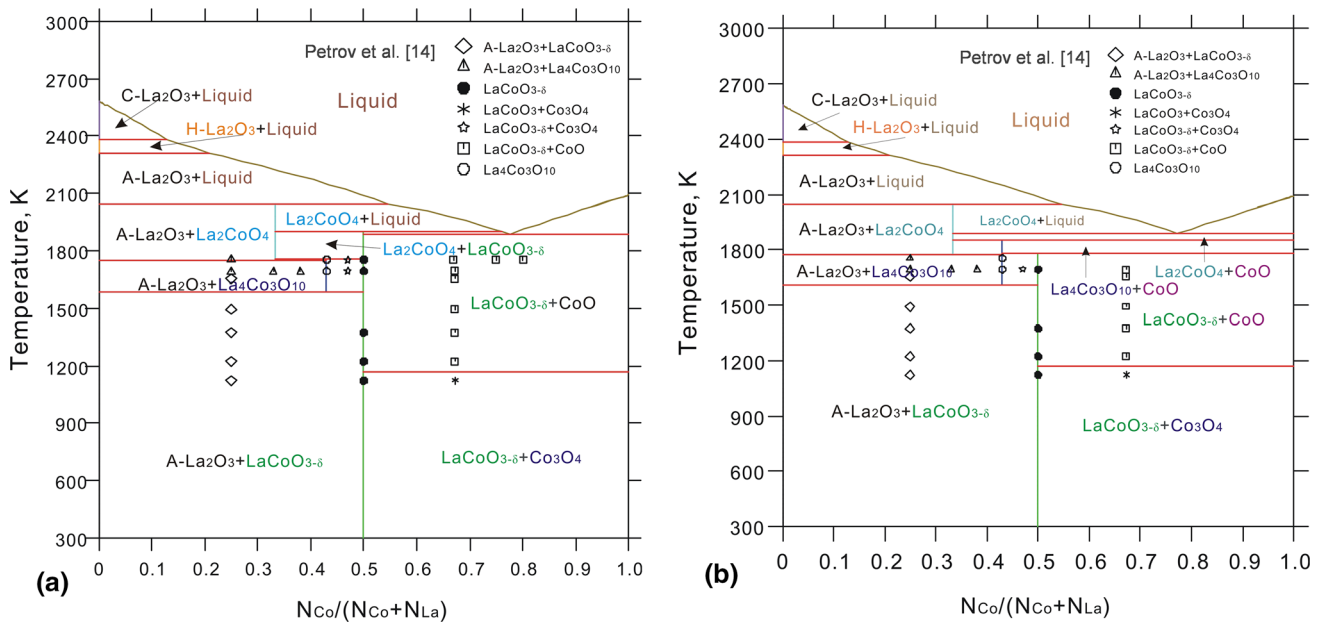
Fig. 4 Calculated phase diagrams of La-Co-O in air in comparison with the experimental data.[14] (a) Using *Parameter Set A* (low charge dispropostionation); (b) Using *Parameter Set B* (high charge dispropostionation). *N* represents mole number
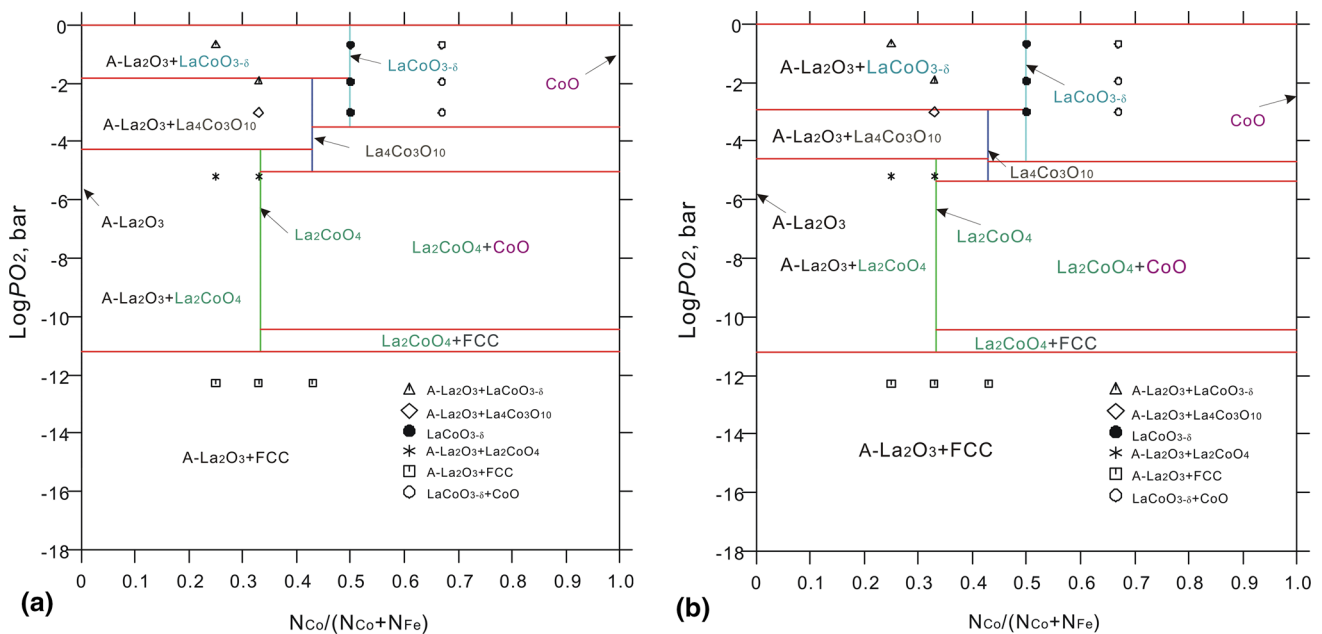

Fig. 5 Calculated isothermal PO_2-composition phase diagrams at 1373 K in comparison with the experimental data from Petrov et al.[14] (a) Using *Parameter Set A* (low charge dispropostionation); (b) Using *Parameter Set B* (high charge dispropostionation)

phases under certain temperature and oxygen partial pressure.

4.3 Oxygen Nonstoichiometry in LaCoO$_{3-\delta}$

The predominant defects in LaCoO$_{3-\delta}$ are oxygen vacancies with $[V_O^{\cdot\cdot}] \propto PO_2^{-1/2}$.[30] Two kinds of situation may

happen in LaCoO$_{3-\delta}$: The electronic defects are localized as valency defects, or defect electrons are delocalized in the conduction band. Petrov et al.,[14,31] used two different models to analyze the defect property of LaCoO$_{3-\delta}$. Model 1 is for itinerant electrons and Model 2 is for localized electrons and holes. Both models fit the experimental data equally well.[14] Based on the oxygen nonstoichiometry

Table 4 Calculated temperatures for various invariant reactions at $PO_2 = 1$ Pa

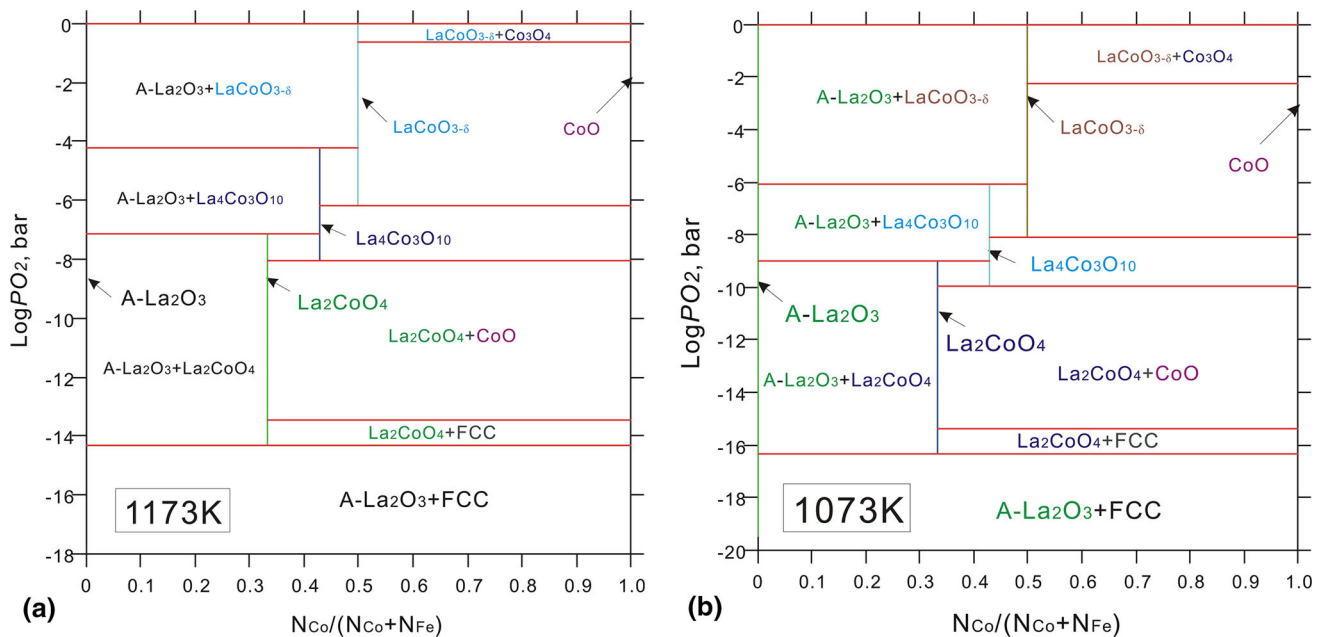| Invariant reactions	Using parameter Set A (T, K)	Using parameter Set B (T, K)
$2La_2CoO_4 + CoO + 1/2O_2 = La_4Co_3O_{10}$	1370	1403
$La_4Co_3O_{10} + CoO + 1/2O_2 = 4LaCoO_3$	1242	1351
$3La_2CoO_4 + 1/2O_2 = La_4Co_3O_{10} + La_2O_3$	1310	1343
$2La_4Co_3O_{10} + 1/2O_2 = 6LaCoO_3 + La_2O_3$	1116	1221

Fig. 6 Calculated isothermal PO_2-composition phase diagrams at different temperatures using *Parameter Set A*: (a) 1173 K, (b) 1073 K

data, it is difficult to conclude whether the high charge disproportionation or the low charge disproportionation reflects the reality.

Figure 8, 9, 10, 11, 12, and 13 present the calculated oxygen deficiency (δ) in $LaCoO_{3-\delta}$ as a function of PO_2 or temperature for single phase $LaCoO_{3-\delta}$ or equilibrated with CoO or La_2O_3. The experimental data can be reproduced equally well using any of the two sets of the parameters. It is therefore difficult to judge whether the high or the low charge disproportionation is the true picture for $LaCoO_{3-\delta}$, just based on the oxygen nonstoichiometry data. However, even though the high charge disproportionation is possible at temperatures from 1000 to 1300 K as shown in Fig. 1, unlikely Co^{3+} will disappear completely. In this sense, the results of Goodenough[33] and Abbate et al.[35] are more reliable. Thus, it was decided that *Parameter set A* with low charge disproportionation will be used for higher order systems. The charge distribution at different temperatures and PO_2 will give a sign to the magnetic properties, electronic conductivity and thermal-

conductivity. Therefore, the knowledge of both the phase equilibria and the charge distribution as a function of the conditions during sample synthesis is decisive for optimization of the manufacturing process.

5 Conclusions

In the present work, the experimental data for the La-Co-O system were carefully reviewed. Thermodynamic modeling of the oxide phases was performed in order to reproduce experimentally determined thermodynamic and phase diagram data. Besides parameter refinements of the stoichiometric $La_4Co_3O_{10}$ phase, the chemical evolution of lanthanum cobaltite was a main issue. We found tight interrelation between oxygen nonstoichiometry and charge disproportionation between the different Co-valence states. Two distinctive sets of optimized model parameter sets can take into account both of the suggested cation schemes of the perovskite phase, i.e. negligible and high extent of the
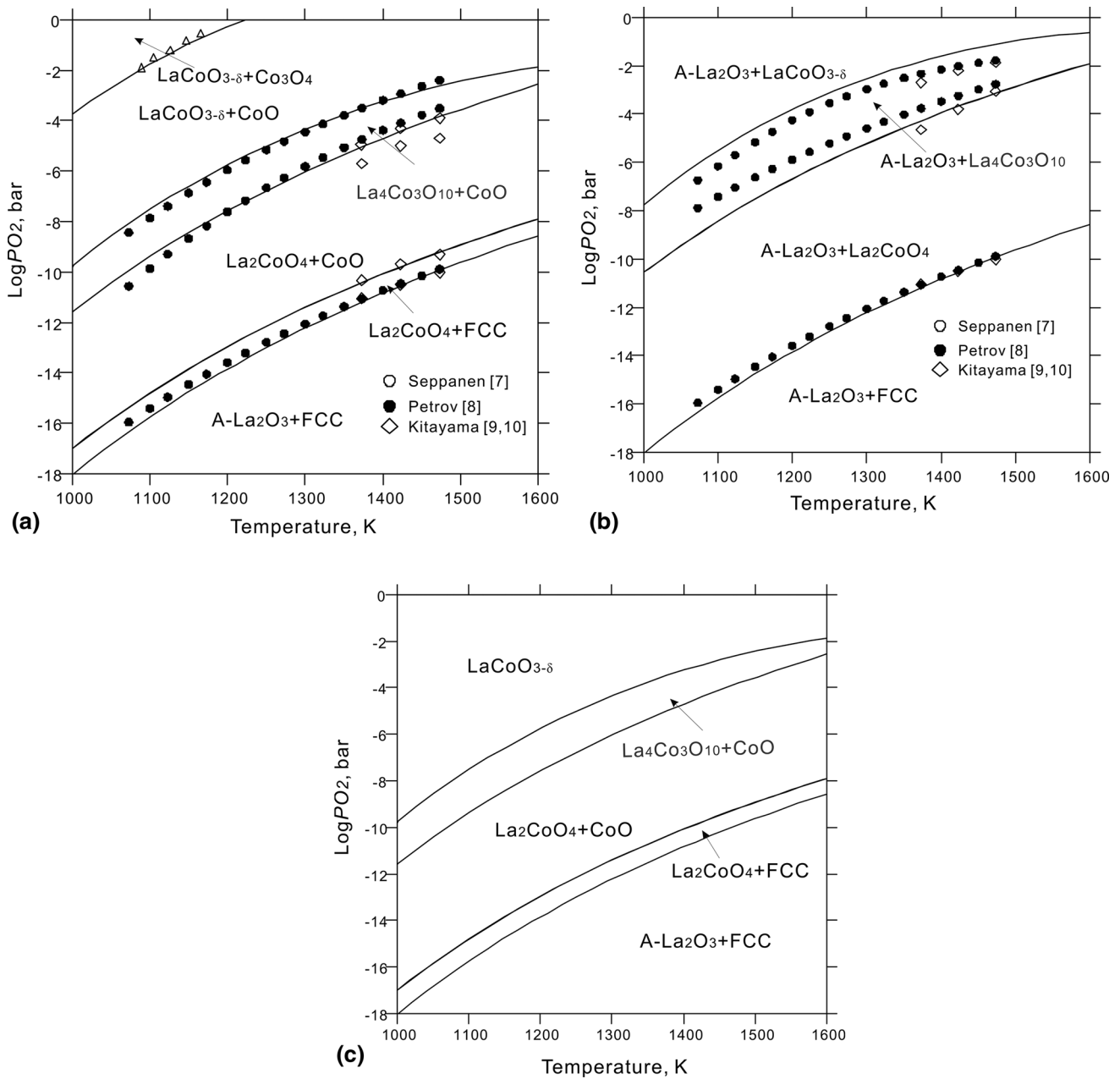
Fig. 7 Calculated stability diagrams of LaO_x-CoO_y using *Parameter Set A* in comparison with experimental data. (a) $x(Co)/(x(Co) + x(La)) =$ 0.7; (b) $x(Co)/(x(Co) + x(La)) = 0.3$; (c) $x(Co)/(x(Co) + x(La)) = 0.5$. x represents mole fraction

disproportionation reaction. *Parameter Set A* allows low charge disproportionation in the perovskite phase, while *Parameter Set B* allows high charge disproportionation. Both sets of parameters can reproduce most of the experimental data equally well. For higher order systems, it is recommended to use *Parameter Set A* with low charge disproportionation. The parameters for $La_4Co_3O_{10}$ phases were also optimized. Our database can be used for calculating phase equilibria and thermodynamic properties at temperatures of 298-3000 K and oxygen partial pressure of $10^{-20} - 1$ bar, and therefore enables material composition optimization for various applications, including SOFC and oxygen membrane.

Fig. 8 Calculated oxygen deficiency (δ) in LaCoO$_{3-\delta}$ as a function of logPO_2 in comparison with experimental data.[30] (a) Using *Parameter Set A*, (b) Using *Parameter Set B*
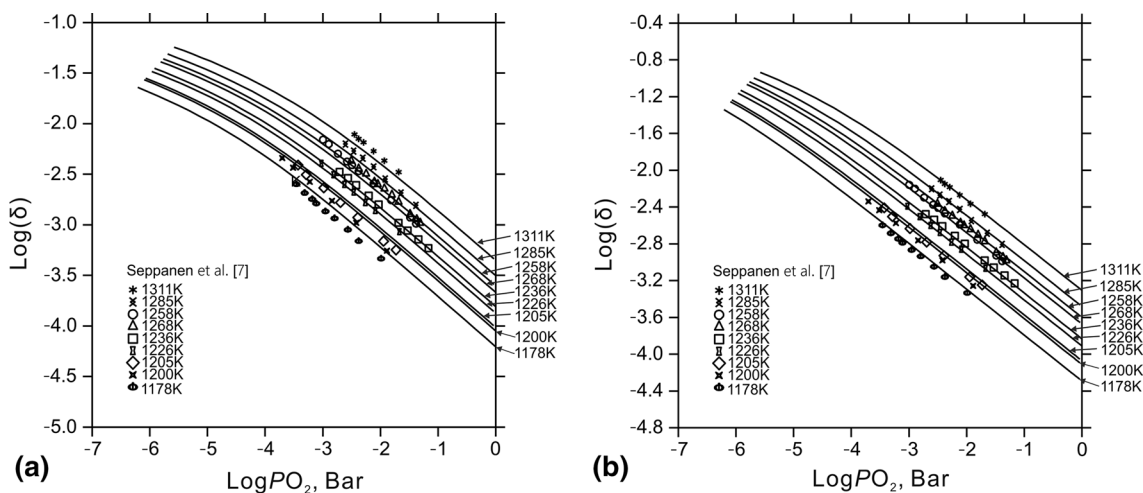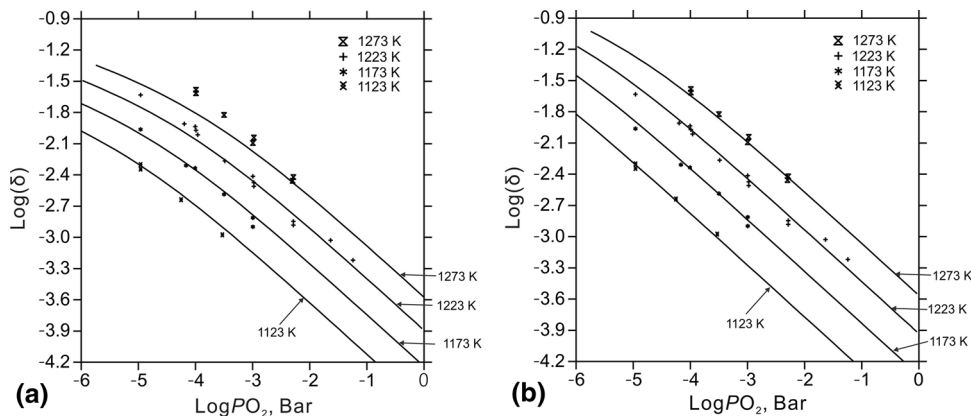

Fig. 9 Calculated oxygen deficiency (δ) in LaCoO$_{3-\delta}$ as a function of logPO_2 together with experimental data.[30] (a) Using *Parameter Set A*, (b) Using *Parameter Set B*

Fig. 10 Calculated oxygen deficiency (δ) in LaCoO$_{3-\delta}$ equilibrated with CoO as a function of logPO_2 compared with experimental data.[29] (a) Using *Parameter Set A*, (b) Using *Parameter Set B*
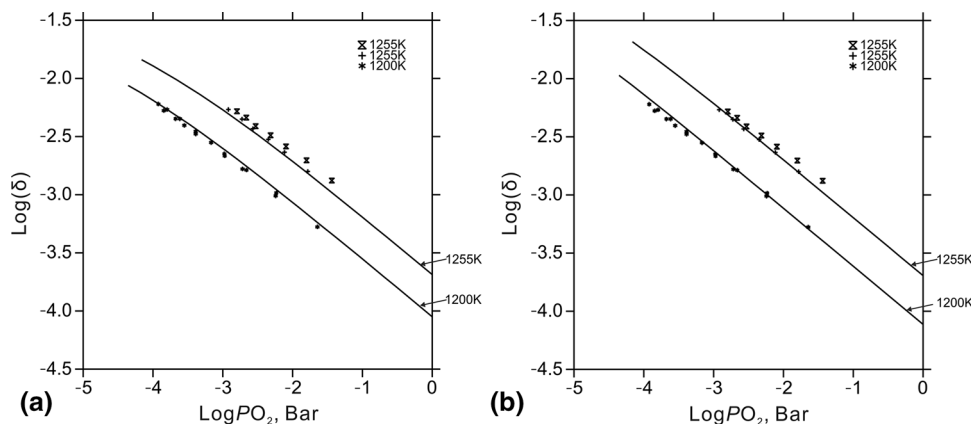
232

J. Phase Equilib. Diffus. (2019) 40:219–234

Fig. 11 Calculated oxygen deficiency (δ) in LaCoO$_{3-\delta}$ equilibrated with La$_2$O$_3$ as a function of logPO_2 in comparison with experimental data.[29] (a) Using *Parameter Set A*, (b) Using *Parameter Set B*
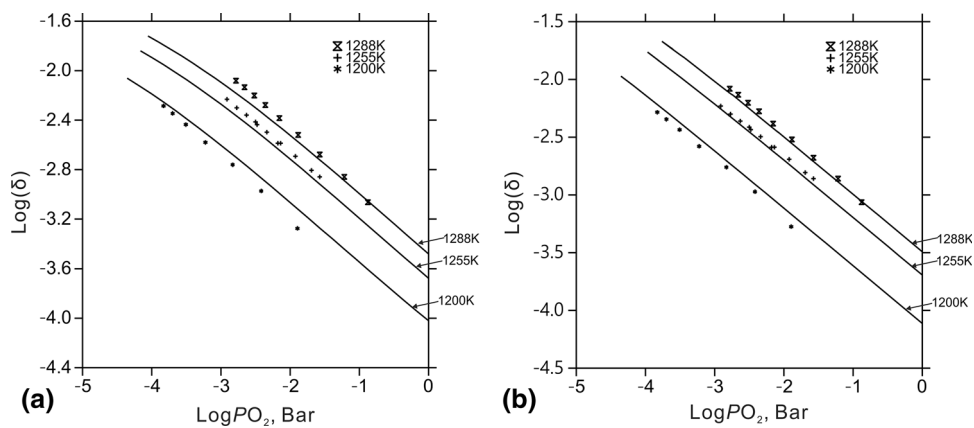

Fig. 12 Calculated oxygen deficiency (δ) in LaCoO$_{3-\delta}$ in air as a function of temperature in comparison with experimental data.[31] (a) Using *Parameter Set A*, (b) Using *Parameter Set B*
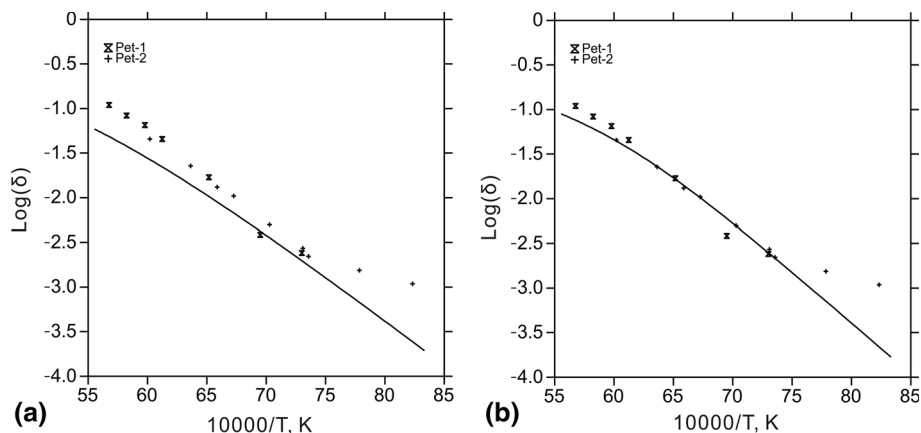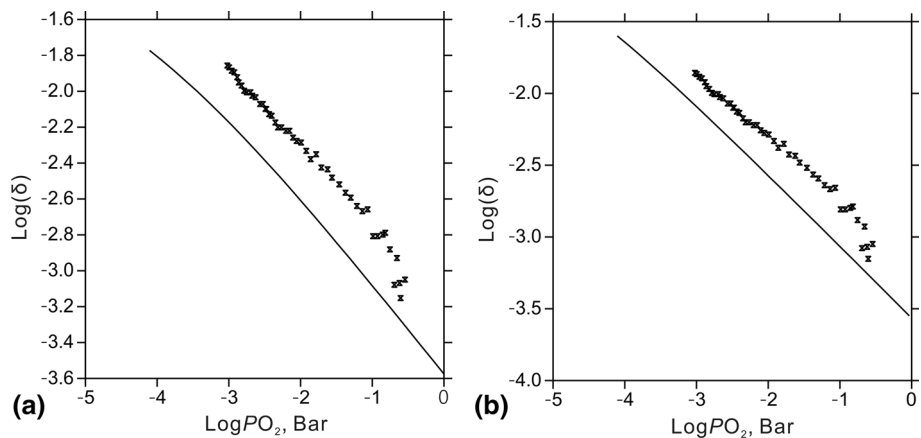

Fig. 13 Calculated oxygen deficiency (δ) in LaCoO$_{3-\delta}$ at 1273 K in comparison with the experimental data from Zuev et al.[32] (a) Using *Parameter Set A*, (b) Using *Parameter Set B*

References

1. S.C. Parida, Z. Singh, S. Dash, R. Prasad, and V. Venugopal, Standard Molar Gibbs Energies of Formation of the Ternary Compounds in the La-Co-O System Using Solid Oxide Galvanic Cell Method, *J. Alloys Compd.*, 1999, **285**(1–2), p 7-11

2. S. Tao, J.T.S. Irvine, and J.A. Kilner, An Efficient Solid Oxide Fuel Cell Based upon Single-Phase Perovskites, *Adv. Mater.*, 2005, **17**(14), p 1734-1737

3. D.B. Meadowcroft, Electronically-Conducting, Refractory Ceramic Electrodes for Open Cycle MHD Power Generation, *Energy Convers.*, 1968, **8**(4), p 185-190

4. L.B. Sis, G.P. Wirtz, and S.C. Sorenson, Structure and Properties of Reduced LaCoO3, *J. Appl. Phys.*, 1973, **44**(12), p 5553-5559

5. J.J. Janecek and G.P. Wirtz, Ternary Compounds in the System La-Co-O, *J. Am. Ceram. Soc.*, 1978, **61**(5–6), p 242-244

6. T. Nakamura, G. Petzow, and L.J. Gauckler, Stability of the Perovskite Phase LaBO3 (B = V, Cr, Mn, Fe Co, Ni) in Reducing Atmosphere I. Experimental Results, *Mater. Res. Bull.*, 1979, **14**(5), p 649-659

7. M. Seppänen, M. Kyto, and P. Taskinen, Stability of the Ternary Phases in the La-Co-O System, *Scand. J. Metall.*, 1979, **8**, p 199-204

8. A.N. Petrov, V.A. Cherepanov, A.Y. Zuyev, and V.M. Zhukovsky, Thermodynamic Stability of Ternary Oxides in Ln-M-O (Ln = La, Pr, Nd; M = Co, Ni, Cu) Systems, *J. Solid State Chem.*, 1988, **77**(1), p 1-14

9. K. Kitayama, Thermogravimetric Study of the Ln2O3-Co-Co2O3 System: I. Ln = La, *J. Solid State Chem.*, 1988, **73**(2), p 381-387

10. K. Kitayama, Thermogravimetric Study of the Ln2O3-Co-Co2O3 System: V. Ln = Nd at 1100 and 1150°C, *J. Solid State Chem.*, 1998, **137**(2), p 255-260

11. N.V. Proskurina, V.A. Cherepanov, O.S. Golynets, and V.I. Voronin, Phase Equilibria and Structure of Solid Solutions in the La-Co-Fe-O System at 1100°C, *Inorg. Mater.*, 2004, **40**(9), p 955-959

12. M. Yang, Y. Zhong, and Z.K. Liu, Defect Analysis and Thermodynamic Modeling of LaCoO3−δ, *Solid State Ion.*, 2007, **178**(15–18), p 1027-1032

13. J.E. Saal, Thermodynamic Modeling of Phase Transformations and Defects: From Cobalt to Doped Cobaltate Perovskites (Ph.D. thesis). The Pennsylvania State University, 2010.

14. A.N. Petrov, V.A. Cherepanov, and A.Y. Zuev, Thermodynamics, Defect Structure, and Charge Transfer in Doped Lanthanum Cobaltites: An Overview, *J. Solid State Electrochem.*, 2006, **10**(8), p 517-537

15. A.N. Grundy, B. Hallstedt, and L.J. Gauckler, Thermodynamic Assessment of the Lanthanum-Oxygen System, *J. Phase Equilib.*, 2001, **22**(2), p 105-113

16. M. Chen, B. Hallstedt, and L.J. Gauckler, Thermodynamic Assessment of the Co-O System, *J. Phase Equilib.*, 2003, **24**(3), p 212-227

17. J.J. Janecek and G.P. Wirtz, The La-Co-O Phase Diagram, *Am. Ceram. Soc. Bull.*, 1975, **54**, p 739

18. M. Seppänen and M.H. Tikkanen, On the Compound Lanthanum Cobalt Oxide (La4Co3O10), *Acta Chem. Scand. A*, 1976, **30**(5), p 389-390

19. O.H. Hansteen and H. Fjellvåg, Synthesis, Crystal Structure, and Magnetic Properties of La4Co3O10+δ (0.00 ≤ δ ≤ 0.30), *J. Solid State Chem.*, 1998, **141**(1), p 212-220

20. U. Lehman and H. Müller-Buschbaum, Ein Beitrag zur Chemie der Oxocobaltate(II): La2CoO4, Sm2CoO4, *Z. Anorg. Allg. Chem.*, 1980, **470**(1), p 59-63

21. J. Lewandowski, R.A. Beyerlein, J.M. Longo, and R.A. McCauley, Nonstoichiometric K2NiF4-Type Phases in the Lanthanum-Cobalt-Oxygen System, *J. Am. Ceram. Soc.*, 1986, **69**(9), p 699-703

22. O.M. Sreedharan and R. Pankajavalli, Standard Gibbs' Energy of Formation of La2CoO4 and Comparison of Stability of La2MO4 (M = Cu, Ni or Co) Compounds, *J. Mater. Sci. Lett.*, 1984, **3**(5), p 388-390

23. Y. Kobayashi, T. Mitsunaga, G. Fujinawa, T. Arii, M. Suetake, K. Asai, and J. Harada, Structural Phase Transition from Rhombohedral to Cubic in LaCoO3, *J. Phys. Soc. Jpn.*, 2000, **69**, p 3468-3469

24. O.M. Sreedharan and M.S. Chandrasekharaiah, Phase Change and Free Energy of Formation of LaCoO3 by Galvanic Cell Method, *Mater. Res. Bull.*, 1972, **7**(10), p 1135-1141

25. O.M. Sreedharan and M.S. Chandrasekharaiah, Standard Gibbs' Energy of Formation of LaFeO3 and Comparison of Stability of LaMO3 (M = Mn, Fe, Co or Ni) Compounds, *J. Mater. Sci.*, 1986, **21**(7), p 2581-2584

26. S. Stølen, F. Grønvold, H. Brinks, T. Atake, and H. Mori, Heat Capacity and Thermodynamic Properties of LaFeO3 and LaCoO3 from T = 13 K to T = 1000 K, *J. Chem. Thermodyn.*, 1998, **30**, p 365-377

27. J. Cheng, A. Navrotsky, X.D. Zhou, and H.U. Anderson, Enthalpies of Formation of LaMO3 Perovskites (M = Cr, Fe Co, and Ni), *J. Mater. Res.*, 2005, **20**(1), p 191-200

28. K. Horinouchi, Y. Takahashi, and K. Fueki, Heat Capacities of LaCoO3 and La0.5Sr0.5CoO3 from 80 to 950 K, *Yogyo-Kyokai-Shi*, 1981, **89**(2), p 104-106

29. M. Seppänen, M. Kyto, and P. Taskinen, Defect Structure and Nonstoichiometry of LaCoO3, *Scand. J. Metall.*, 1980, **9**(1), p 3-11

30. J. Mizusaki, Y. Mima, S. Yamauchi, K. Fueki, and H. Tagawa, Nonstoichiometry of the Perovskite-Type Oxides La1−xSrxCoO3−δ, *J. Solid State Chem.*, 1989, **80**(1), p 102-111

31. A.N. Petrov, V.A. Cherepanov, and A.Y. Zuev, Oxygen Nonstoichiometry of Lanthanum, Praseodymium and Neodymium Cobaltates with Perovskite Structure, *Russ. J. Phys. Chem.*, 1987, **61**, p 326-330

32. A.Y. Zuev, A.N. Petrov, A.I. Vylkov, and D.S. Tsvetkov, The Oxygen Nonstoichiometry and Defect Structure of Unsubstituted LaCoO3−δ Cobaltite, *Russ. J. Phys. Chem.*, 2007, **81**(1), p 73-77

33. J.B. Goodenough, Narrow-Band Electrons in Transition-Metal Oxides, *Czechoslov. J. Phys.*, 1967, **17**(4), p 304-336

34. V.G. Bhide, D. Rajoria, and Y.S. Beddy, Localized-to-Itinerant Electron Transitions in Rare-Earth Cobaltates, *Phys. Rev. Lett.*, 1972, **28**(17), p 1133-1136

35. M. Abbate, J.C. Fuggle, A. Fujimori, L.H. Tjeng, C.T. Chen, R. Potze, G.A. Sawatzky, H. Eisaki, and S. Uchida, Electronic Structure and Spin-State Transition of LaCoO3, *Phys. Rev. B*, 1993, **47**(24), p 16124-16130

36. M.A. Korotin, S.Y. Ezhov, I.V. Solovyev, and V.I. Anisimov, Intermediate-Spin State and Properties of LaCoO3, *Phys. Rev. B*, 1996, **54**(8), p 5309-5316

37. M.W. Haverkort, Z. Hu, J.C. Cezar, T. Burnus, H. Hartmann, M. Reuther, C. Zobel, T. Lorenz, A. Tanaka, N.B. Brookes, H.H. Hsieh, H.J. Lin, C.T. Chen, and L.H. Tjeng, Spin State Transition in LaCoO3 Studied Using Soft X-ray Absorption Spectroscopy and Magnetic Circular Dichroism, *Phys. Rev. Lett.*, 2006, **97**, p 176405

234

J. Phase Equilib. Diffus. (2019) 40:219–234

38. Z. Hu, H. Wu, M.W. Haverkort, H.H. Hsieh, H.J. Lin, T. Lorenz, J. Baier, A. Reichl, I. Bonn, C. Felser, A. Tanaka, C.T. Chen, and L.H. Tjeng, Different Look at the Spin State of Co^{3+} Ions in a CoO_5 Pyramidal Coordination, *Phys. Rev. Lett.*, 2004, **92**(20), p 207402

39. G. Maris, Y. Ren, V. Volotchaev, C. Zobel, T. Lorenz, and T.T.M. Palstra, Evidence for Orbital Ordering in $LaCoO_3$, *Phys. Rev. B*, 2003, **67**, p 224423

40. H. Yokokawa, T. Kawada, and M. Dokiya, Construction of Chemical Potential Diagrams for Metal-Metal-Nonmetal Systems: Applications to the Decomposition of Double Oxides, *J. Am. Ceram. Soc.*, 1989, **72**(11), p 2104-2110

41. A.N. Grundy, B. Hallstedt, and L.J. Gauckler, Experimental Phase Diagram Determination and Thermodynamic Assessment of the La_2O_3–SrO System, *Acta Mater.*, 2002, **50**(9), p 2209-2222

42. E. Povoden, A.N. Grundy, M. Chen, T. Ivas, and L.J. Gauckler, Thermodynamic Assessment of the La-Fe-O System, *J. Phase Equilib. Diffus.*, 2009, **30**(4), p 351-366

43. C.P. Wang, J. Wang, X.J. Liu, I. Ohnuma, R. Kainuma, and K. Ishida, Thermodynamic Assessment of the Co-La and Mo-La Systems, *J. Alloys Compd.*, 2008, **453**(1–2), p 174-179

44. S.V. Ushakov and A. Navrotsky, Direct Measurements of Fusion and Phase Transition Enthalpies in Lanthanum Oxide, *J. Mater. Res.*, 2011, **26**(7), p 845-847

45. M. Zinkevich, Thermodynamics of Rare Earth Sesquioxides, *Prog. Mater Sci.*, 2007, **52**(4), p 597-647

46. Mats Hillert, The Compound Energy Formalism, *J. Alloys Compd.*, 2001, **320**(2), p 161-176

47. A.T. Dinsdale, SGTE Data for Pure Elements, *Calphad*, 1991, **15**(4), p 317-425

48. G. Inden, Determination of Chemical and Magnetic Interchange Energies in BCC Alloys. I. General Treatment, *Z. Met.*, 1975, **66**(10), p 577-582

49. M. Hillert and M. Jarl, A Model for Alloying in Ferromagnetic Metals, *Calphad*, 1978, **2**(3), p 227-238

50. M. Hillert, B. Jansson, B. Sundman, and J. Ågren, A Two-Sublattice Model for Molten Solutions with Different Tendency for Ionization, *Metall. Trans. A*, 1985, **16**(1), p 261-266

51. B. Sundman, Modification of the Two-Sublattice Model for Liquids, *Calphad*, 1991, **15**(2), p 109-119

52. M. Zinkevich, S. Geupel, F. Aldinger, A. Durygin, S.K. Saxena, M. Yang, and Z.K. Liu, Phase Diagram and Thermodynamics of the La_2O_3-Ga_2O_3 System Revisited, *J. Phys. Chem. Solids*, 2006, **67**(8), p 1901-1907

53. S.G.T.E. Thermodynamic Properties of Inorganic Materials, volume 19 of Landolt–Börnstein New Series, Group IV (Springer, Berlin, 1999)

54. A.N. Grundy, M. Chen, B. Hallstedt, and L.J. Gauckler, Assessment of the La-Mn-O System, *J. Phase Equilib. Diffus.*, 2005, **26**(2), p 131-151

55. E. Povoden, M. Chen, A.N. Grundy, T. Ivas, and L.J. Gauckler, Thermodynamic Assessment of the La-Cr-O System, *J. Phase Equilib. Diffus.*, 2009, **30**(1), p 12-27

56. E. Povoden, M. Chen, T. Ivas, A.N. Grundy, and L.J. Gauckler, Thermodynamic Modeling of La_2O_3-SrO-Mn_2O_3-Cr_2O_3 for Solid Oxide Fuel Cell Applications, *J. Mater. Res.*, 2012, **27**(15), p 1915-1926

57. J.-O. Andersson, T. Helander, L. Höglund, P. Shi, and B. Sundman, Thermo-Calc & DICTRA, Computational Tools for Materials Science, *Calphad*, 2002, **26**(2), p 273-312

Publisher's Note Springer Nature remains neutral with regard to jurisdictional claims in published maps and institutional affiliations.